Ductile Fracture Initiation in Braces of Concentrically Braced Frames

Tamilselvan Nambirajan, Viresh Singh, and P. C. Ashwin Kumar

Abstract Braces in concentrically braced frame system dissipate majority of the seismic energy imparted to the structure through inelastic cyclic axial deformations. During the inelastic cyclic deformations, the braces might initiate fracture prematurely if the selection of the brace geometry is not decided properly. Hence, the main objective of the study is to couple the continuum-level study with micro-mechanical fracture model to decipher the localized mechanism behind the origin of brace fracture initiation phenomenon. Monotonic and cyclic notched bar test results available in the literature have been used to calibrate the numerical model for capturing the inelastic cyclic material response. The calibrated numerical model has then been used to model the braces across a wide range of brace geometries, using which the stress and strain histories for cyclic loading have been evaluated. The evaluated stress and strain histories with the help of micro-mechanical fracture model have been used to capture the ductile fracture initiation of braces. From the obtained results, it has been observed that the slenderness ratio and width to thickness ratio have a strong influence over the initiation of ductile fracture in braces.

Keywords Passive devices · Ductile fracture initiation · Slenderness ratio · Stress triaxiality · Equivalent plastic strain · Low cycle fatigue

T. Nambirajan (✉) · P. C. A. Kumar
Indian Institute of Technology, Roorkee, India
e-mail: ntamilselvan@eq.iitr.ac.in

P. C. A. Kumar
e-mail: ashwin.pc@eq.iitr.ac.in

V. Singh
Indian Institute of Technology, Tirupati, India
e-mail: ce17b026@iittp.ac.in

M. Madhavan et al. (eds.), *Proceedings of the Indian Structural Steel Conference 2020 (Vol. 1)*, Lecture Notes in Civil Engineering 318,
https://doi.org/10.1007/978-981-19-9390-9_9

1 Introduction

Steel braces are designed as a sacrificial element in a concentrically braced frame (CBF) to dissipate the seismic energy imparted to the structure during earthquakes. Premature fracture in braces has been found to be detrimental to the global performance of the structure during a seismic event [2]. Hence, it is imperative that the inelastic cyclic performance of braces including the fracture phenomenon needs to be studied thoroughly. Till now, many studies [5, 6, 8, 15] have been conducted to capture the inelastic behavior and predict the fracture initiation point of steel braces subjected to reversed cyclic displacements. These studies observed that the high strains and rotations generated at the corners of compressive side, located at the middle of the brace, caused fracture after one to four cycles of local buckling. These high inelastic strains generated in the middle region are due to concentration of tensile elongation in the post-buckling stage. Accurate modeling of braces and capturing the micro-mechanical changes are thus necessary to capture these stress concentration and local buckling effects. Few recent studies have used both micro-mechanics-based method and accurate numerical modeling to predict fracture initiation [5, 6]. Among these studies, the cyclic void growth model (CVGM-extended model of void growth model) by Kanvinde et al. [7] has been found to be most accurate. The parameters like stress triaxiality and equivalent plastic strain incorporated in this model enable to capture complex interactions of stress–strain histories. Thus, the main objective of this study is to correlate the fracture initiation point with the collapse assessment study of steel braces. The corresponding validation of the fracture model and the effects of slenderness ratio and width to thickness ratio of braces on the fracture initiation are evaluated in this study.

2 Objective and Scope of Study

The objective of this study is mainly focused on developing numerical model of hollow square steel (HSS) braces and to accurately capture stress–strain histories at maximum stress concentrated point and to apply the principles of CVGM to predict the fracture initiation point. The validation of the process, including the method and the numerical model, is sought through the results obtained from a previous study [5]. The validated numerical model is then utilized to find the influence of slenderness ratio and width to thickness ratio on prediction of fracture initiation point. Six specimens with three HSS braces of same slenderness ratio but varying width to thickness ratio and other three with same width to thickness ratio with varying slenderness ratio have been modeled for this study. The selected HSS brace specimens are as given in Table 1.

Table 1 Brace details considered in this study

B (mm)	t (mm)	SR	B/t
SET 1			
203.2	9.5	37	10.8
203.2	15.9	39	19.9
177.8	3.2	42	57
SET 2			
355.6	22.2	22	14.2
76.2	4.8	102	
50.8	3.2	153	

3 Element Model Description

Steel braces are modeled using S4R (four node quadrilateral shell element) elements in ABAQUS v6.14 (2014). The reduced integration element possesses six degree of freedom per node and three translational and three rotational degrees. Distribution of stress nonlinearity has been estimated by adopting seven integration points along the element thickness. Local buckling and brace fracture (through micro-mechanics-based method) have also been captured using this element. The middle of the brace where plastic hinge is expected is densely meshed, and at location away from the center, the mesh sizes have been gradually increased (Fig. 1a). For the regions in the gusset plate where yielding is expected, fine mesh has been provided (Fig. 1b) to explicitly include the response due to out of plane buckling effect of brace under cyclic loading. Interface nodes have been used to connect the gusset plate with HSS specimens. Since the final failure response desired in this study is the fracture of the brace at the middle, weld detailing between gusset plate and brace has not been considered in the numerical model. The brace numerical model has been provided with fixed (rigid)-end boundary conditions at the ends of the gusset plates. Since the cyclic performance of steel braces highly depends on the dimensions of gusset plate and connections detailing [12], their effects have been accounted in the model to determine the effect of slenderness ratio on prediction of fracture initiation point of HSS braces. The gusset plate for all study specimens have been designed using the balanced design procedure developed by Roeder et al. [12]. The balanced design procedure provides the required brace ductility level through incorporation of inelastic deformation of gusset plate and also takes cares of the yielding hierarchy of braces and gusset plates.

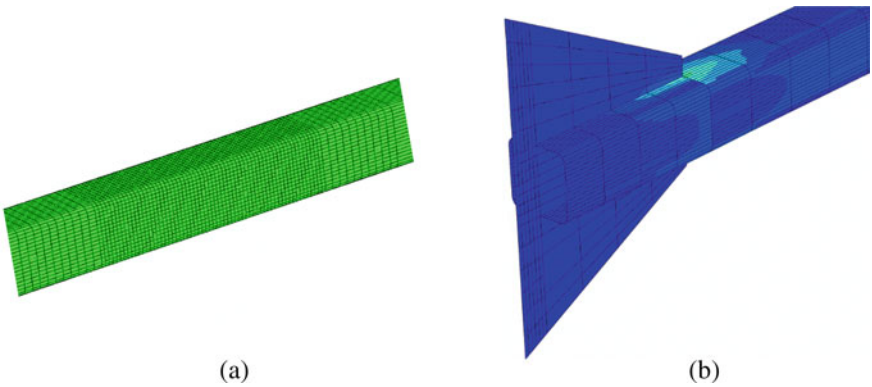

Fig. 1 Mesh pattern of **a** Brace mid-length and **b** Gusset plate

3.1 Material Properties

The assumption of von-Mises yield criterion has been used to determine the material yielding using the finite element model of steel braces used in this study. This assumptions have been found to be satisfied by most of the metals [4]. The yield surface growth is captured by isotropic hardening model; however, this fails to include (1) the effect of cold working anisotropic behavior and (2) effect of local stress generation due to internal dislocation of atoms along one direction during cyclic loading. Therefore, for exact consideration of (1) all shifts and volume change of yield surface in three-dimensional stress space, (2) to evaluate the functional influence of stress at yield stage on inelastic loading protocol, and (3) the influence of cyclic behavior of metals on loading history, the HSS brace model has been supported with combined hardening material model (both isotropic and kinematic hardening). The definition of the yield surface for a combined hardening material model is given using Eq 1.,

$$f(\sigma_{ij}, k) = \left[\frac{3}{2}(S_{ij} - \alpha_{ij}^{d})(S_{ij} - \alpha_{ij}^{d})\right]^{1/2} - \sigma_{y_0} - k = 0 \tag{1}$$

where σ_{ij} represents the stress tensor; S_{ij} represents the back stress tensor that possesses a deviatoric part α_{ij}^{d}; and σ_{y0} represents the initial yield stress with k as the hardening parameter defining the yield surface size.

The purely kinematic hardening yielding surface function can be obtained by putting $k = 0$ in Eq. (1). On the other hand, by making the deviatoric part as zero, we can get the yielding surface function for pure isotropic hardening. Different inelastic or plastic hardening models [3, 16] can be used to subtract the yield surface shift from the respective stresses. Among them, the Ziegler's kinematic hardening rule [16] has been found to possess the capacity of shifting the yield surface in three-dimensional stress space for the model used in this study. Correspondingly, the nonlinear kinematic hardening component can be divided into two terms: (1) linear

kinematic term conforming with the Ziegler hardening law and (2) to introduce nonlinearity, back stress term is used that can be expressed by the function given in Eq. (2).

$$\alpha_k = C_k \frac{1}{\sigma_0}(\sigma - \alpha)\varepsilon^p - \gamma_k \alpha_k \varepsilon^p \tag{2}$$

where σ^0 represents the initial yield stress; ε^p represents the equivalent plastic strain rate; and C_k and γ_k represent the initial kinematic hardening modulus and its rate of variation corresponding to the incremental variation of inelastic deformation. The back stress developed is represented by α, which is expressed by the function given in Eq. (3),

$$\alpha = \sum_{k=1}^{N} \alpha_k \tag{3}$$

where the term N represents the quantity of back stress used. The effect of hardening and softening of the material has been taken into account by the isotropic hardening component expressed as a function of equivalent plastic strain ε^p given by Eq. (4),

$$\sigma^0 = \sigma^0(\varepsilon_p) = \overline{\sigma}_0 + Q_\infty(1 - e^{-b\varepsilon_p}) \tag{4}$$

where $\vec{\sigma}_0$ represents the yield stress corresponding to zero plastic strain; Q_∞ represents maximum growth in yield surface size; and b represents the growing rate of yield surface size with plastic strain increment. The present study utilizes the values of yield stress and combined hardening parameters obtained from a previous study [5]. In this previous study, the standard tension coupon test has been used to provide the yield stress value σ_y. The isotropic and kinematic hardening parameters have been evaluated by using circumferentially large notched cyclic test and small smooth notched monotonic test. The parameters obtained have been compared and refined slightly with the numerical model of coupon notched test. The parameters used for small-scale elements have been then applied to numerical models of large-scale braces, which are then verified with the experimental results. These hardening parameters thus obtained may vary slightly with the dimensions and shape of the brace section used and do not represent a unique value for a particular grade of material. However, in this study, a constant single value of these parameters has been assumed (Table 2), which have been taken directly from [5].

3.2 Simulating Global Buckling Behavior

ANSI/AISC 341-16 [1] provisions corresponding to slenderness ratio and width to thickness ratio have been considered in the selection of brace sizes to be used in this

Table 2 Calibrated hardening parameters [5]

Element	σ_y (Pa)	C (MPa)	γ	Q_∞ (MPa)	b
Brace corner	503	5861	160	100	5.25
Brace wall	469	2069	25	69	6
Gusset plate	345	3448	38	118	5

study. Fracture initiation of braces mainly depends on the strain development at the stage of local and global buckling of braces. Both the stages have to be accurately captured by the numerical model for significant prediction of fracture initiation point. With regard to capturing the initial imperfection and out of straightness effect of brace, an elastic analysis has been carried out to capture the mode shapes. Scaled eigenvector of the first mode (global buckling of brace) has been used to perturb the brace while being loaded axially. To simulate the brace buckling, the initial perturbation magnitude has been provided as 0.001 L, where L is the brace length. For capturing of local buckling, no extra perturbation has been provided.

3.3 Loading Protocol

The study of Fell [5] on the loading protocol revealed that the ground motions of far-field earthquakes are highly critical for assessing the performance of steel braces in comparison with the ground motions representing near field earthquakes. Thus in this study, the standard cyclic loading protocol provided by the guidelines of ATC-24 (1992) provisions has been followed. Loading protocol provided by ATC-24 (1992) has been obtained from the investigation of nonlinear dynamic analyses of many ductile moment frame systems. For accurate capturing of braced frame response, the selected loading protocol has been modified according to the suggestions provided by Krawlinker et al. [9, 10]. The modified loading protocol is as given in Fig. 2.

The initial elastic steps in the loading protocol are followed by four cycles representing the onset of brace buckling initiation under compressive loading cycle. As a whole, nine steps of loading cycle have been provided with the maximum deformation of braces corresponding to five percent story drift [14]. The story drift has been related to the axial deformation of steel braces by Eq. (5) as,

$$\Delta_a = \left(\cos^2 45^\circ\right) L_B \theta \tag{5}$$

where Δ_a represents the brace axial deformation, L_B is brace effective length, and θ is the brace inter-story drift angle. Equation (5) is only valid for chevron type of brace configuration with an inclination of brace to the horizontal as 45°. The effect of (1) influence of flexural deformation of beams and columns and (2) panel zone deformation on the cyclic behavior of steel braces has not been accounted in this study.

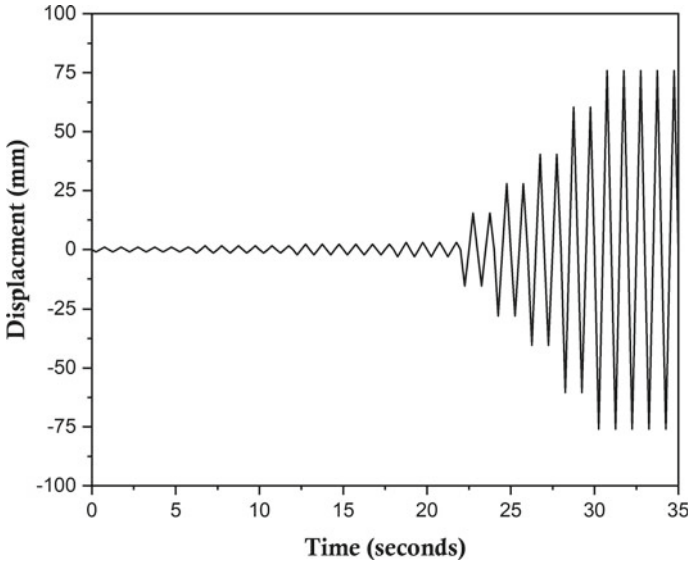

Fig. 2 Modified standard loading protocol used in this study

3.4 Selection of Brace Section

The upper limiting value of slenderness ratio (SR) for steel brace used in SCBFs according to the ANSI/AISC 341-16 [1] provision is 200. Hence, three SRs 22, 102, and 153 have been chosen for this study. To determine the effect of slenderness ratio (SR), three SRs of 22, 102, and 153 with fixed *B/t* ratio of 14.2 have been selected for this study. To evaluate the effect of width to thickness ratio on fracture initiation of braces, three *B/t* ratios 10, 19.9, and 57 for fixed SR near to 40 have been selected in this study. The limiting value of width to thickness ratio provided by ANSI/AISC 341-16 [1] is as given in Eq. 6,

$$\left(\frac{B}{t}\right)_{\max} = 0.65\sqrt{\left(\frac{E}{F_y}\right)} \tag{6}$$

The section width is considered as (B-3t) in the calculation of width to thickness ratio. The upper limit of *B*/*t* for steel with Young's modulus of 200 GPa and fy (yield stress of steel brace wall) of 486 MPa is found to be 13.2. The *B*/*t* ratio for some sections has been intentionally selected beyond the limit to evaluate the effect of local buckling and different SR on fracture initiation of braces. The *B*/*t* ratios (within limit) 10, (on border of upper limit) 14.2, and (far beyond the upper limit) 57 with same SR nearly to 40 have been selected to evaluate the effect of limiting width to thickness ratio on fracture initiation of braces. The selected brace section with its properties is given in Table 1. All sections have a constant length of 2946 mm. This

constant length system assumption in this study fits well with the practical design cases, where the fixed brace length exists due to constant floor height of the building.

4 Cyclic Void Growth Model

Traditional fracture model have very limited accuracy on fracture initiation prediction of steel subjected to cyclic loading. These model works on the assumption that the crack already exists in the material. Moreover, extensive inelastic yielding that occurs under cyclic loading brings extra inaccuracy to the traditional fracture models. Low cycle fatigue of steel braces under reversed axial displacements makes the steel braces more vulnerable to earthquakes. To reduce the vulnerability, the fracture initiation of steel braces has to be evaluated accurately under cyclic type of loading. Rice and Tracey [13] using the micro-mechanism of void growth and coalescence provided an empirical relation to predict fracture initiation of steel under monotonic loading. Kanvinde et al. [7] extended the void growth model (VGM) for the application of VGM under cyclic loading and termed it as cyclic void growth model (CVGM).

When the monotonic degradation capacity is less than the demand cyclic growth, fracture in steel braces is initiated, and the above phenomenon is given as

$$\exp\left(-\lambda_{\mathrm{CVGM}}\varepsilon_p\right)\eta_{\mathrm{monotonic}} \leq \sum_{\text{Tensile - cycles}} \int_{\varepsilon_1}^{\varepsilon_2} \exp(|1.5T|)\mathrm{d}\varepsilon_t - \sum_{\text{compressive - cycles}} \int_{\varepsilon_1}^{\varepsilon_2} \exp(|1.5T|)\mathrm{d}\varepsilon_c \quad (7)$$

The CVGM depends on two factors: (1) stress triaxiality (T) and (2) equivalent plastic strain (ε_p). The tensile cycles are represented by positive *T,* and compressive cycles are represented by negative T. The intersection of critical void growth index (VGI) (degradation of monotonic capacity) and cyclic VGI (demand cyclic growth) decides the fracture initiation point as shown in Fig. 3.

5 Analysis Results

The influence of slenderness ratio and width to thickness ratio (within, near, and beyond the upper limit) on prediction of fracture initiation is evaluated from the post processed results of validated numerical model and discussed in the following sections.

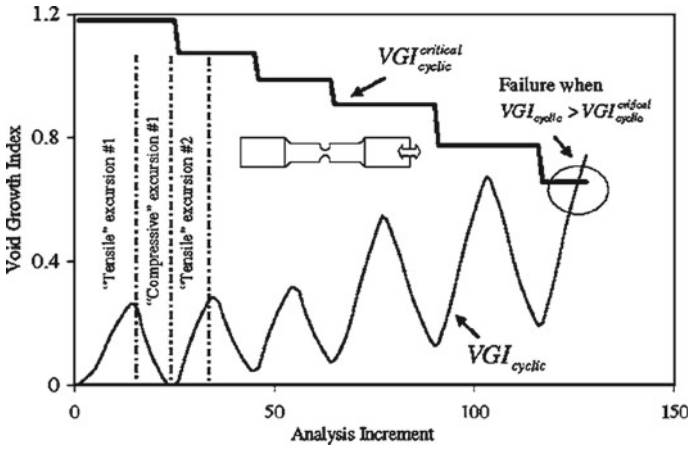

Fig. 3 Graphical representation of prediction of fracture initiation in steels

5.1 Validation of Numerical Model

The numerical model developed in this study is first validated with the results of experiment conducted by Fell [5]. Geometry, loading protocol, and material properties have been kept exactly same as the experiment conducted.

The validated hysteresis response of steel brace is shown in Fig. 4a. Even though there is a slight variation in the hysteresis, the critical stages, i.e., the onset of global and local buckling, matched accurately. The last loading cycles of numerical model continue even after the fracture of brace because no ductile damage model has been fed into the numerical model. Local buckling of steel brace with high width to thickness and low SR is shown in Fig. 4b. The stress and strain histories obtained from the maximum stressed point in the numerical model have been processed with CVGM substituting the constants $\lambda_{\text{CVGM}} = 0.17$ and $\eta_{\text{monotonic}} = 5.98$ taken from Fell [5] in Eq. (7) to predict the fracture initiation point. The obtained fracture initiation point has then been compared with the results of Fell [5]. It is found that the numerical model predicts the fracture initiation one loading step before the results of Fell [5] as shown in Fig. 5a. This prior prediction of fracture initiation is mainly due to the effect of mesh sensitivity and localized behaviour in the plastic hinge region developed in the middle of the brace section. Figure 5b shows the monotonic degradation capacity, cyclic demand growth obtained from the numerical model used, and the fracture initiation point with the respect to loading time step.

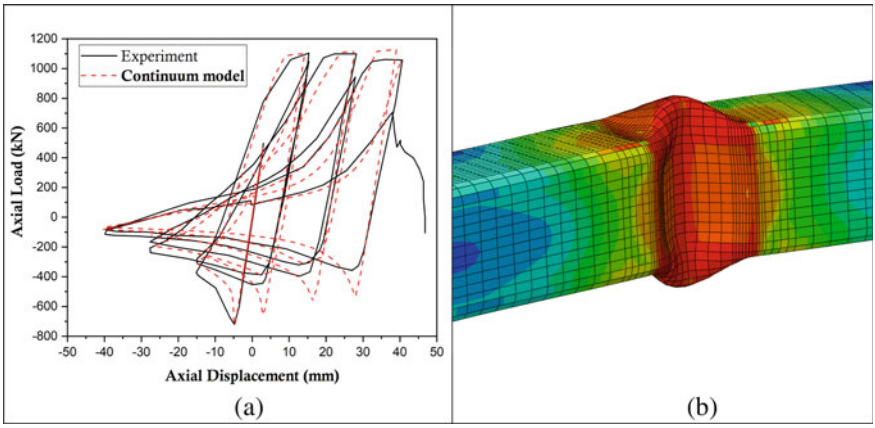

Fig. 4 **a** Comparison of hysteresis response. **b** Local buckling at half-length plastic hinge region

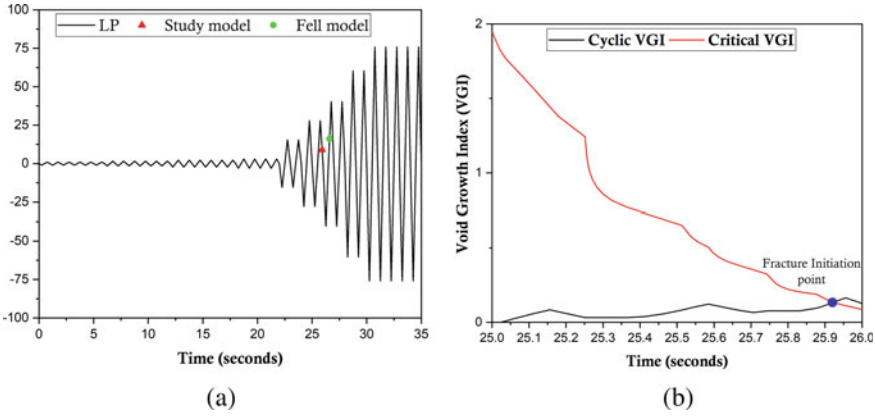

Fig. 5 **a** Comparison of fracture initiation prediction. **b** Graphical representation of intersection of critical VGI and cyclic VGI obtained from continuum model

5.2 *Influence of Width to Thickness Ratio on Fracture Initiation Prediction*

Set 1 given in Table 1 consists of sections with varying width to thickness ratio selected in an order of being within the upper limit, near to the upper limit, and far beyond the upper limit and having almost equal SR. The fracture predicted in all the three sections is as given in Fig. 6a. It can be observed that the upper limit provided by ANSI/AISC 341-16 [1] delays the fracture initiation in steel braces. *B/t* of 19.9 and 10 fractured nearly at same drift cycle. The fracture initiation for *B/t* of 57 is observed in the tensile loading cycle at a drift of 2%, and for other two *B/t* ratio of

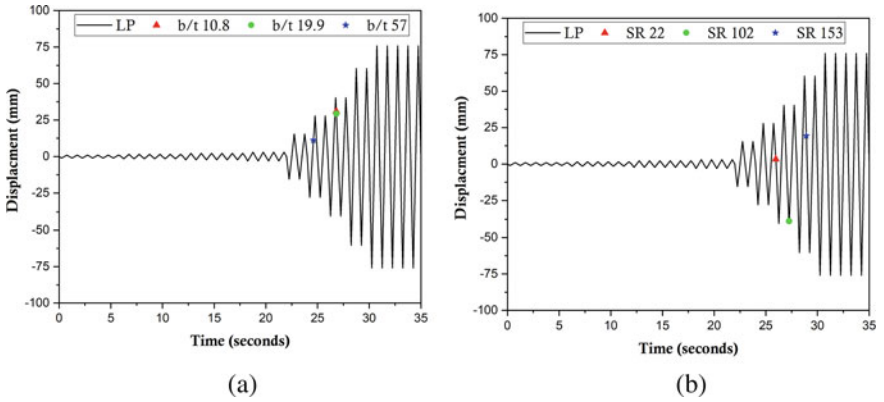

Fig. 6 Variation in fracture initiation for **a** different width to thickness ratio **b** different slenderness ratio

10 and 19.9, it is observed in the tensile unloading cycle at a drift of 3%. The early fracture of brace with larger B/t ratio is in line with past research results.

5.3 Influence of Slenderness Ratio on Fracture Initiation Prediction

Set 2 given in Table 1 consists of section with varying slenderness ratio of 22, 102, and 153 with constant *B/t* of 14.2. The influence of slenderness ratio on prediction of fracture initiation is shown in Fig. 6b. It is observed that increase in SR delays the fracture initiation in steel braces. Also low SR with high *B/t* ratio resulted in early fracture initiation in steel braces which matches previous experimental result trends. High SR range initiates fracture at a drift of 4%, whereas the low slenderness initiates fracture at 2%, respectively.

6 Conclusions

The numerical model validated with the experiment conducted by Fell [5] has been used to validate the CVGM model, and it has then been used to evaluate the influence of SR and *B/t* ratio on prediction of fracture initiation in steel braces. The following conclusions can be drawn from this study:

1. The sensitivity of mesh size, localized effects, and ombined hardening parameters play a major role in accurately predicting the fracture initiation in brace.

2. Numerical model accurately captures the instances of local and global buckling in the braces and in combination with CVGM method predicts the instances of fracture initiation with great accuracy.
3. Early fracture of braces with low slenderness ratio and high *B/t* ratio and delayed fracture in cases of higher slenderness ratio have been captured accurately by the micro-mechanics-based method employed in this study.

References

1. ANSI/AISC 341-16 (2016) Seismic provisions for structural steel buildings. American Institute of Steel Construction, Chicago, IL, p 60601
2. Bruneau M, Uang CM, Whittaker A (2011) Ductile design of steel structures, vol 389. McGraw-Hill, New York
3. Chaboche JL (1986) Time-independent constitutive theories for cyclic plasticity. Int J Plast 2(2):149–188
4. Chen WF (1994) Constitutive equations for engineering materials. Vol. 2 plasticity and modeling. Elsevier
5. Fell BV (2008) Large-scale testing and simulation of earthquake-induced ultra-low cycle fatigue in bracing members subjected to cyclic inelastic buckling. University of California, Davis
6. Haddad M (2015) Concentric tubular steel braces subjected to seismic loading: finite element modeling. J Constr Steel Res 104:155–166
7. Kanvinde AM, Deierlein GG (2007) Cyclic void growth model to assess ductile fracture initiation in structural steels due to ultra low cycle fatigue. J Eng Mech 133(6):701–712
8. Kumar PA, Sahoo DR (2018) Fracture ductility of hollow circular and square steel braces under cyclic loading. Thin-Walled Struct 130:347–361
9. Krawinkler H (1992) Guidelines for cyclic seismic testing of components of steel structures, vol. 24. Applied Technology Council
10. Krawinkler H, Gupta A, Medina R, Luco N (2000) Loading histories for seismic performance testing of SMRF components and assemblies. SAC Joint Venture, Report no. SAC/BD-00/10. Richmond, CA
11. Manual AU (2014) Abaqus theory guide. Version 6.14. Dassault Systemes Simulia Corp, USA
12. Roeder CW, Lumpkin EJ, Lehman DE (2011) A balanced design procedure for special concentrically braced frame connections. J Constr Steel Res 67(11):1760–1772
13. Rice JR, Tracey DM (1969) On the ductile enlargement of voids in triaxial stress fields∗. J Mech Phys Solids 17(3):201–217
14. Sabelli R, Roeder CW, Hajjar JF (2013) Seismic design of steel special concentrically braced frame systems. NEHRP, Gaithersburg, USA, Seismic Design Technical Brief, 8
15. Shaback B, Brown T (2003) Behaviour of square hollow structural steel braces with end connections under reversed cyclic axial loading. Can J Civ Eng 30(4):745–753
16. Ziegler H (1959) A modification of Prager's hardening rule. Q Appl Math 17(1):55–65